Available online at www.sciencedirect.com
SCIENCE DIRECT®
PERGAMON
International Journal of Heat and Mass Transfer 46 (2003) 4911–4923
International Journal of HEAT and MASS TRANSFER
www.elsevier.com/locate/ijhmt

LDV assisted bubble dynamic parameter measurements from two enhanced tubes boiling in saturated R-134a

Shou-Shing Hsieh *, Wen-Chuan Lai, Huang-Hsiu Tsai

Department of Mechanical and Electro-Mechanical Engineering, National Sun Yat-Sen University, Kaohsiung 80424, Taiwan, ROC

Received 28 October 2002; received in revised form 25 February 2003

Abstract

LDV measurements and heat transfer experiments for nucleate pool boiling from two horizontal enhanced tubes with porous copper on copper surfaces immersed in saturated R-134a were conducted. The influence of tube position (alignment) and tube pitch on bubble dynamics and boiling characteristics were studied. Photographs indicate that the average number of bubbles increases with heat fluxes, which is the same as those in previous studies of single tube. However, the bubble departure diameters of the upper tube show an opposite trend with an increase as compared to previous single-tube studies. LDV measurements show that the present tube arrangement has significant influence on local velocity in both magnitude and trend. The heat transfer mechanism and modeling for the upper tube were studied and developed.

1. Introduction

Many water chillers of the centrifugal type have evaporators utilizing a flood of operation whereby the water is circulated through the tube and the refrigerant evaporated on the shellside of the tubes in nucleate pool boiling. The evaporator tube bundle is fully wetted at full-loaded operating conditions. Most of previous research on nucleate pool boiling heat transfer was directed at the clarification of characteristics for a single tube or on plate as well as the multi-rods results. Even though, neither sufficient experimental data nor reliable methods are available for the prediction of nucleate pool boiling in tube bundles, especially for enhanced tube bundles despite its important application to process heat exchangers.

Early research on heat transfer coefficients in large multi-tube bundles was performed by Palen and coworkers [1–3]. In these studies, only tube-bundle average heat transfer coefficients were obtained, but those coefficients were greater than those for a single tube in saturated pool boiling.

Significant progress has been made in understanding nucleate boiling heat transfer and two-phase convection effects on the shell sides of smooth tube bundles [4–6], either a photographic technique to study the circulation effects in a slice of a reboiler tube bundle or high-speed photography to observe numerous bubbles sliding over and around the top tubes or the influence of two-phase convection effects in a bundle was examined. The influence of tube position within a bundle of smooth tubes has been extensively studied by Fujita et al. [7], finned tube bundles by Muller [8]. Experimental investigation was performed by Jensen et al. [9] to examine the effects of cross-flow on the heat transfer coefficients in a tube bundle with smooth and Wolverine Turbo-B and Linde High Flux enhanced tubes.

Recently, Marto and Anderson [10] made measurements for R-113 nucleate pool boiling for a bundle of 15 electrically heated, smooth copper tubes arranged in an equilateral triangular pitch with a $p/d = 2$, higher heat transfer coefficients of the upper tubes were found. Later, Memory et al. [11] conducted almost the similar work except that a Turbo-B tube bundle was used. Significant enhancement (up to 4.6 at a low heat flux)

* Corresponding author. Tel.: +886-7-525-2000; fax: +886-7-525-4215.
E-mail address: sshsieh@mail.nsysu.edu.tw (S.-S. Hsieh).

0017-9310/$ - see front matter © 2003 Elsevier Ltd. All rights reserved.
doi:10.1016/S0017-9310(03)00351-X

Nomenclature

A	total surface area of test tube, mm^2
A_b	bottom surface area of test tube, mm^2
A_s	side surface area of test tube, mm^2
A_t	top surface area of test tube, mm^2
d	outside diameter of test tube, mm
d_b	bubble departure diameter, mm
f	bubble departure frequency, s^{-1}
h	heat transfer coefficient, W/m^2 K
Nu	Nusselt number, hd_b/K
q	heat flux, W/m^2
q_{cb}	heat flux (bottom surface of the tube) due to onflow vapor flux, W/m^2
q_{cs}	heat flux (side surface) due to onflow vapor flux, W/m^2
q_{ct}	heat flux (top surface) due to onflow vapor flux, W/m^2
T	temperature measured, K
ΔT	temperature difference, K
u	bubble departure valuably, m/s

Subscripts

b	bubble
c	onflow vapor flux
cb	bottom surface
cs	side surface
ct	top surface
1	tube 1
2	tube 2

was found. Li and Hahne [12] experimentally studied the boiling heat transfer on finned tube bundle with lower tubes heated with constant heat flux in R-11 at a pressure of 1 bar. The heat transfer coefficient with a given pitch-to-diameter ratio were increased as much as 150% and the time-averaged liquid velocity under the bubble can be reached to maximum as the heat increases. These studies have employed several photographic techniques to determine the above-stated bubble dynamic data. Few of them have applied the data to predict each component of the total heat flux (latent heat, natural convection, and microconvection) as well as to validate their boiling models.

Barthau [13] proposed an optical method for measuring the active nucleation size density on a tube immersed in R-114 at various pressures. The heat transfer contribution of an individual active site is found to decrease with increasing pressure and to decrease strongly with increasing heat flux. Small increases of the bubble departure diameter and of the bubble frequency have been observed with increasing heat flux. Ammerman et al. [14] developed a unique method to determine the vapor volumetric flow rate as well as boiling dynamic data above a heated wire within a saturated liquid FC-72 utilizing a single photograph and Laser-Doppler anemometry. Overall contributions to the total heat flux from four nucleate boiling heat transfer mechanisms were determined.

In recent years, environmental concerns over the use of CFCs as working fluids in refrigeration and air-conditioning plants have led to the development of alternative fluids. Among these alternatives, R-134a and R-600a are used as substitutes for the commonly used CFC-12. Moreover, considerable effort has recently been made to find ways to design more compact and efficient evaporators for the process and refrigeration industries based on CFCs/non-CFCs. Industries are currently undergoing a massive conversion process from CFC to HFC (like R-134a) or HC (like R-600a). The conversion establishes a need for refrigerant data on the substitute refrigerants such as R-134a used in this study. In spite of foregoing merits, those methods as Barthau [13] and Ammerman et al. [14] have the disadvantage of being limited to either special types of fluids or to special types of heating surfaces. Therefore, more accurate and detailed study of the bubble dynamic data especially for bubble departure velocity from coated enhanced surfaces in R-134a and R-600a are needed. Mertz et al. [15] reported an experimental study for tubes with wires in compact two-phase heat exchangers. Very recently, Hsieh and Ke [16] performed a series of pool nucleate boiling heat transfer experiments from coated surfaces with porous copper (Cu) and molybdenum (Mo) and helically wrapped with wire on copper surfaces immersed in saturated R-134a.

This paper is a continuation of the work of Hsieh and Ke [16] to broaden our fundamental understanding of the mechanisms of pool boiling heat transfer on plasma coated tubes in saturated R-134a.

2. LDV measurements and videography

The present system is a commercial two color, four beam DANTEC fringe-type LDV system, operated in the backward scatter mode, with the general layout shown in Fig. 1, similar to that of Hsieh and Ke [16]. Standard DANTEC 55× modular optics and a model Stabilite 2016 4W Special Physics Ar^+ laser are mounted on a two-dimensional, traversing system. Two separate LDV channels are formed by use of color separation of beams with wavelengths 514.5 nm (green light) and

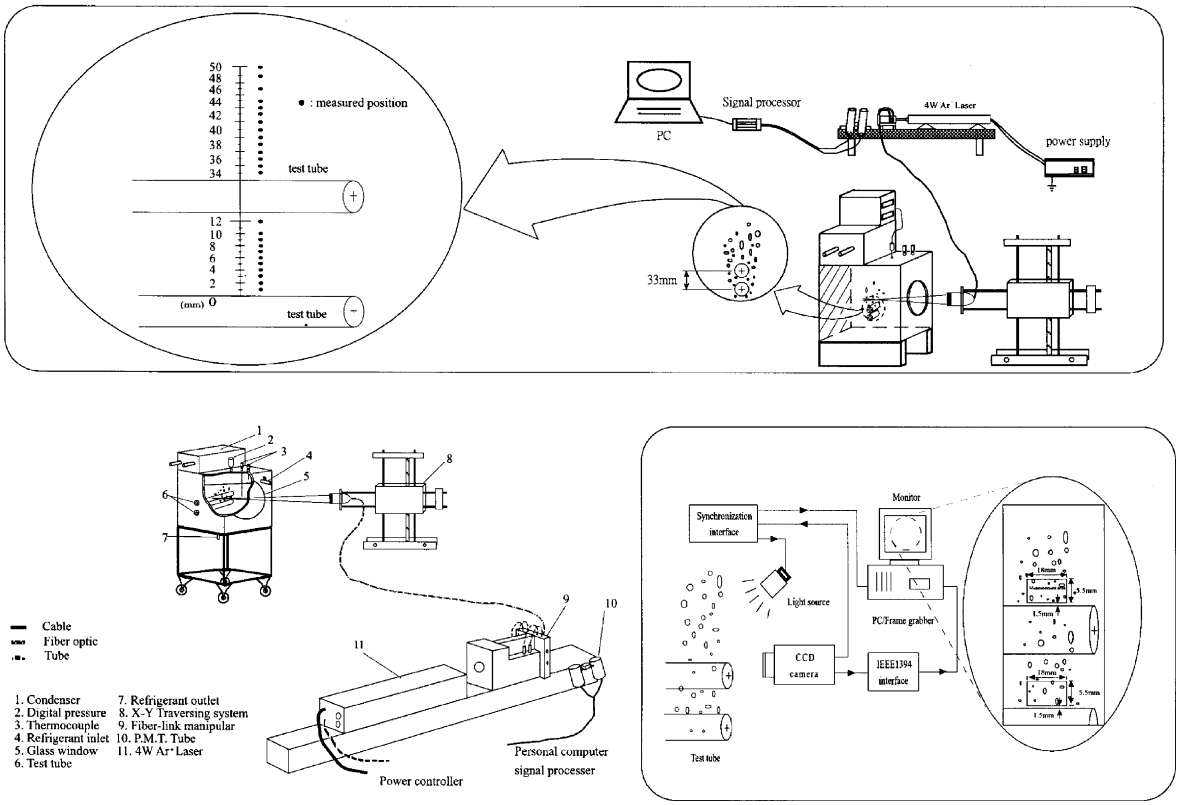

Fig. 1. Photography technique and LDV facility schematic bubble dynamic data.

488.0 nm (blue light). These two beams form orthogonal fringes by means of a standard DANTEC two channel optical train. These two sets of fringes allow the simultaneous measurement of two orthogonal velocity components with 128×128 pixel interrogation areas. The transverse velocity component is measured using the 488.0 nm beam, while the 514.5 nm beam measures a streamwise velocity component. A combined counter-type signal processor (Dantec model 57H00) with functions of counter, buffer interface and coincidence filter, which is interfaced with a LEO (Intel-486) PC in the direct access mode, was employed for data processing. Statistical data were based on a sample size of 320,000 measurements with a sampling frequency of approximately 400 samples/s, from which the time-averaged values were determined.

Various sources of uncertainty contribute to the random and system errors in the mean velocity measurements. These included index of refraction effects that alter the half-angle between the beams and the optical probe volume location; velocity bias, filter bias, and velocity gradient broadening; and finite size of the data samples. The visual optical volume positioning uncertainty was kept less than ±0.01 mm by the careful determination of an initial reference location and using stepping motors with incremental steps equal to 50 μm.

A JVC Model Gr-DVM 70 gated, high resolution CCD video camera with a motion analyzing system was used to visualize the boiling phenomena in the test sections as also shown in Fig. 1. This system was used to capture single-frame images of vapor bubbles above the heated surface, and it can provide images at a speed of 30 frames/s. Such a technique is the same as the work reported by Ammerman et al. [14]. The illumination provide by one LPL-BROM CINE 500 W floodlight was filtered through a diffuser for the videography. The field of view is 18×5.5 mm in the horizontal and vertical directions, respectively. Video images were synchronized and transferred to an IBM 586 PC, where they were digitized by a 640×480 frame grabber board and analyzed by image processing software. There are 11 positions (points) to be measured (one value/measured point) as indicated in Fig. 1. Following Ammerman et al. [14], a single photo method was applied to analyze the present measuring data to obtain the bubble departure diameter. The nucleation site density was measured for different heat fluxes by photographing the test tubes with a high-speed camera at 30 frames/s. The flash duration used was less 50 ns and the camera is capable

of shutter speeds up to 1/500th of a second. The photograph was projected on a screen to obtain sufficient magnification, and the bubbles corresponding to nucleation sites on the surface were thus counted.

3. Experiment

The basic experimental apparatus used in the study is shown in Fig. 1. It consisted of an evaporator and condenser arranged to provide reflux operation. A rectangular vessel, 370 mm in width, 650 mm in height, and 370 mm in depth, with an electrically heated two-tube bundle was used R-134a was used as the working fluid. Both tubes were made from commercially available, 20 mm dia smooth copper tubing with porous copper coated. The tubes were cantilever mounted from the back wall of the evaporator to permit observation of the boiling phenomena along the axis of tubes through two glass windows mounted in the rear and side of Fig. 2. The tubes in the bundle were arranged in vertical-in-line configuration with a definite pitch of 1.65 depicted in Table 1.

Fig. 2 is a schematic sectional view of the test section that shows the sets of tubes. Each heated tube contained 1 kW electrical cartridge heaters, 11.1 mm o.d. with a heated length of 220 mm. Two auxiliary heaters, each capable of 1.5 kW, were installed on the front side of the test bundle to maintain the liquid pool at saturated conditions and to provide system pressure control. Also, the heated tubes were instrumented with thermocouples at four circumferential positions in the middle for sur-

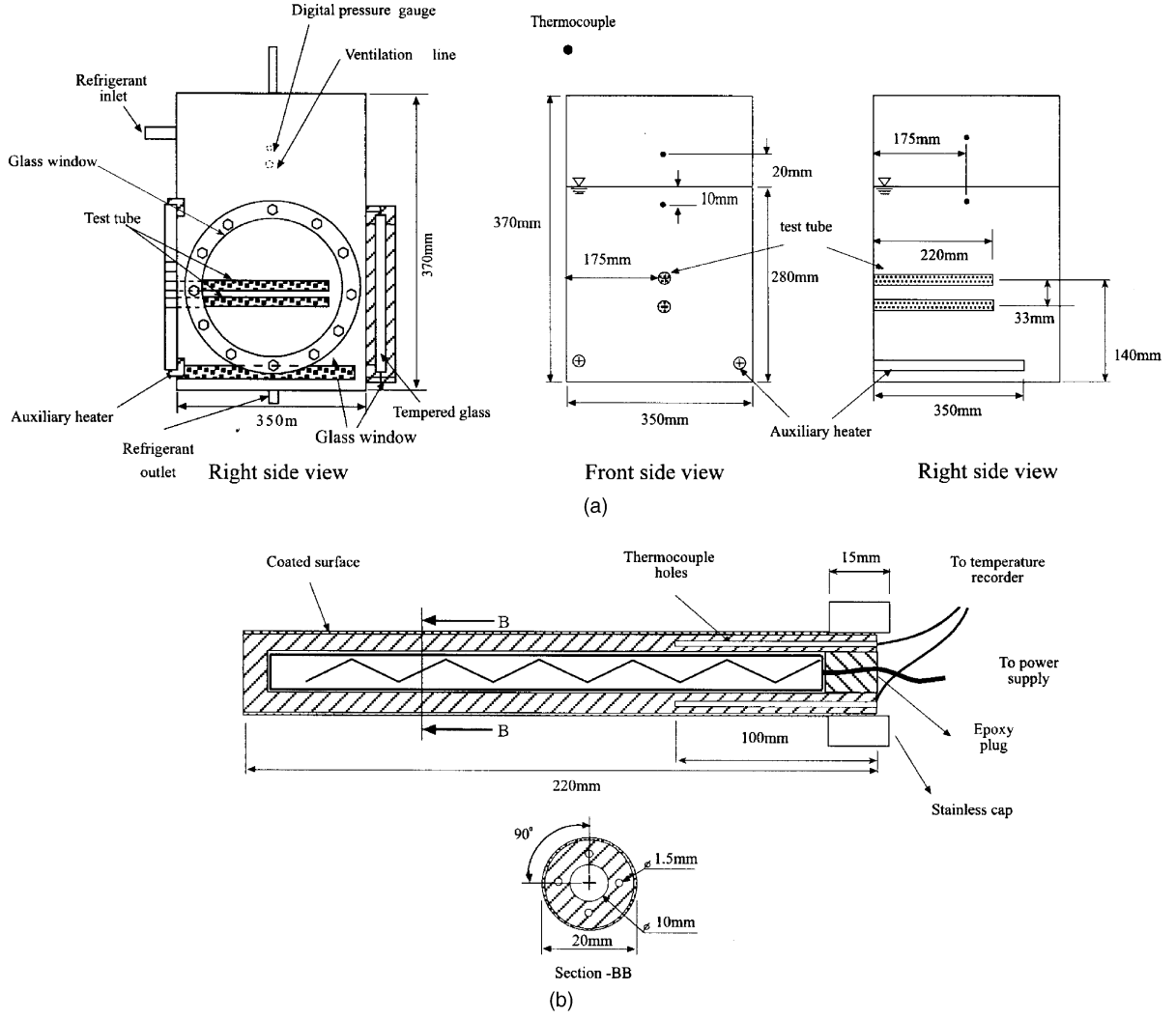

Fig. 2. (a) Test section; (b) thermocouple positions and test specimen.

Table 1
The specification and dimensions of the present coated tubes studies

Tube	Smooth tube	Plasma tube (Cu)
Surface (coating material)	Smooth	Cu
Thickness of porous layer (μm)	–	100
Surface roughness (μm)	0.07	7.84
Porosity (μm)	–	0.057
Mean pore diameter (μm)	–	4

Note: All tubes considered have OD 20 mm and ID 10 mm with a length 200 mm.

face temperature measurements. Four slots were machined into the sheath as shown in Fig. 2(b). The slots extended from one end to about 1/3 length of the heater exposed junction stainless steel sheath (1.5 mm o.d.), four type T thermocouples (1.1 mm o.d.) were placed into the slots to measure the circumferential temperatures (at four equidistant locations along the periphery). Each slot was then press fitted with an aluminum filler piece welded, and machined to restore a smooth surface. The power to the heaters was supplied by a 110 V, 30 A, DC power supply.

Experiments reported in the present paper were performed using R-134a as the boiling liquid. R-134a has a boiling point of 18 °C at the pressure of 537.06 kPa. Data were obtained by both increasing and decreasing heat flux in steps and taking measurements when the steady-state was reached. Steady-state was determined when temperature variations between the adjacent two tubes/or for the single tube is less than ±0.2 °C for 2 min.

In order to study the bundle effects on the boiling characteristics systematically, experiments were performed on two, vertical-in-line tubes.

The enhanced surface were prepared by the method described by Hsieh and Yang [16]. Because the heater surface roughness significantly influences the boiling behavior, it was examined using an atomic force microscope (AFM) as well as a scanning electron microscope (SEM). Fig. 3(a) and (b) show two typical AFM scans (50 and 80 μm) from the side of coated surfaces, and the top as well as side view for SEM, respectively. The topography and 3-D feature of the surface condition can be clearly seen in Fig. 3(a). Fig. 3(b) shows a rather random distribution of cavities and pores of varying shapes and sizes along the heated surface. The resultant surface condition is also listed in Table 1. Prepared test sections were cleaned with chlorinol and water and finally, with acetone. The tank was cleaned with acetone before each run. Once the evaporator tube bundle had been installed, the system was evacuated to a pressure of about 30 Pa. If no leaks were detected over a 24 h interval, the evaporator was charged with the working fluid from a reservoir to a level of 60 mm above the top of the upper tube. This resulted in a vapor pressure of 537.06 kPa (R-134a).

Power was applied to the pool to degas the test fluids. R-134a at heat flux of 10 kW/m^2 for 1.5 h. The saturation temperature at the measured pressure was compared to the pool temperature measured by the thermocouple. The power supplied to the test section was gradually, and slowly, reduced to zero. The test pool was maintained close to the saturation temperature with an auxiliary heater for about 40 min; then it was switched off to minimize convective effects. The heating power supplied to the test section was slowly and gradually increased to nearly 10 kW/m^2.

During all the tests, the saturation temperature was kept near 18 °C for R-134a supplied by ICI. The liquid level was kept approximately 100 mm above the test tube. All the data were obtained and reduced with a computer-controlled data acquisition system.

The precautions taken during experiments are summarized as following:

1. The pool temperature was compared to the saturation temperature corresponding to the measured saturation pressure for refrigerants, This ensures that there are no non-condensibles in the container. It also verifies that there is no subcooling in the liquid pool within ±0.2 K.
2. To ensure that the correct wall temperature was measured, a tightly pressed thermocouple was put onto the wall of a sleeve insert with thermal jointing compound applied to the tube. In addition, a three-dimensional heat transfer model was employed to correct the wall temperature measured (i.e., to minimize the conductance and capacitance effect) to obtain a more accurate (or nearly true) wall temperature. Consequently, 0.1 K accuracy was expected.
3. The heater was tested for circumferential uniformity of heat flux. Non-uniformities in the heat flux were smoothed out followed the methodology described in Hsieh and Ke [16].

4. Data reduction and uncertainty analysis

For each power input, the heat transfer coefficient was calculated on the basis of bulk fluid saturation temperature (T_{sat}), tube heat flux (q), and the average value (T_{avg}) of the four tube wall temperatures. The heat transfer coefficient at each power input was then calculated, following $h = Q/[A(T_{avg} - T_{sat})]$ forth upper/level tubes.

Using the method of Kline and McClintock [12], uncertainty estimates were made considering the errors of the instruments, the measurement variance, geometry uncertainty and calibration errors for the heat flux,

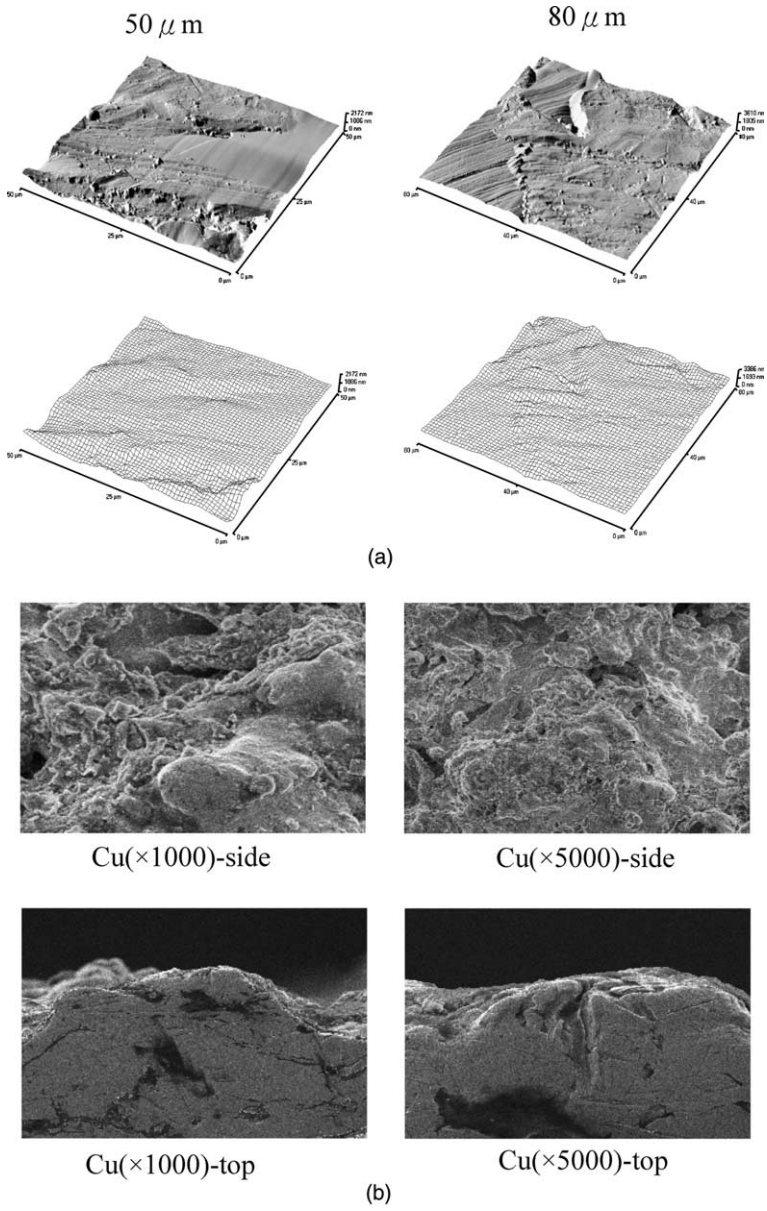

Fig. 3. (a) AFM and (b) SEM photographs of enhanced tube microstructure.

temperature, and bubble dynamic parameter measurements. The uncertainty in the wall superheat was dominated by the uncertainty in the wall temperature measurements. The values of the four wall temperatures were recorded and compared to examine variation caused either by non-uniformities in the cartridge heater or by the test tube soldering and assembly procedure. Wall superheat uncertainty can be attributed primarily to thermocouple calibration (±0.1 °C) and temperature correction from the thermocouple reading to the reference surface. The maximum variation of the four measured wall temperatures was ±0.2 °C at the maximum heat flux (≅10 kW/m^2). The uncertainty in the saturation temperature was estimated to be less than ±0.2 °C.

Substrate conduction heat losses were quantified at different heat flux conditions by solving three-dimensional conduction problems with a finite-difference solver. This loss varied between 10.2% and 2% for heat flux conditions between 0.8 and 10 kW/m^2, respectively. The other primary contributor to heat flux uncertainty was heated surface area. For instance, it is about ±4% for Tube 3 (Cu) coated surface at $q = 0.8$ kW/m^2. Com-

Table 2
Maximum possible measurement errors

Quantity	Systematic error	Random error
ΔT	◯ ±0.37% ◎ ±0.36%	◯ ±0.38% ◎ ±0.35%
q	◯ ±9.49% ◎ ±1.44%	◯ ±9.66% ◎ ±2.18%
d_b	◯ ±1.40% ◎ ±0.44%	◯ ±1.30% ◎ ±0.35%
h	◯ ±9.50% ◎ ±1.48%	◯ ±9.66% ◎ ±2.20%
d	±0.003%	±0.025%
f	±8%	±5%
T	±1.7%	±1.5%
x	±0.05 mm	±0.01 mm
y	±0.05 mm	±0.01 mm
z	±0.05 mm	±0.01 mm
u	±2.5%	±0.4%

Note: ◯ 500 W/m^2; ◎ 10 000 W/m^2.

bining these effects lead to overall uncertainty estimates in heat flux of 11.2% at the lowest heat input. Based on these uncertainties, it indicates the uncertainty of the wall heat transfer coefficient to be about ±15% at $q = 0.8$ kW/m^2.

Accuracy of the bubble diameter measurements is estimated to be within ±1.9% or ±0.6% at the minimum/or maximum heat flux with an extreme high space resolution (~9.5 nm) of CCD camera. The uncertainty in the number of bubbles was found within ±7.1% for the minimum and ±4.9% for the maximum heat flux. Uncertainty estimates for time is ±1.7%. The frequencies reported are average values and observed fluctuations in frequency are less than ±0.8%. The data presented refer to individual and isolated bubbles. Of the uncertainties specifically attributable to the LDA technique, filter bias, velocity bias, and gradient broadening were carefully examined. Filter bias was avoided. The maximum velocity bias was estimated to be less than 10% but typically, it was about 10%. The effect of gradient broadening seems negligible. Calculation of the mean results in statistical uncertainties of ±12% for mean velocity at the largest heat flux level. Table 2 summarizes the estimates of maximum inaccuracy (systematic error) and imprecision (random error) associated with each measurements.

5. Results and discussion

Experimental results for two plasma coated tubes arranged with two tube pitches ($p/d = 1.65$ and 2.5) were conducted at low and modest heat fluxes ($q \leqslant 10$ kW/m^2) for boiling visualization ($q \leqslant 1$ kW/m^2) and LDV as well as heat transfer measurements.

5.1. Boiling visualization

The photographs shown in Fig. 4 are the bubble occurrence, departure, and growth for the tube with plasma coating at $600 \leqslant q \leqslant 1000$ W/m^2 in saturated R-134a for $p/d = 1.65$. The effect of onflow due to the lower tube to the upper tube seems to be clearly noted for the size and the velocity of the bubbles. The bubble agglomeration and coalescence are significant as compared to that for a single tube (see Hsieh and Ke [16]). There are filled with vapor in the present study. In addition, more vigorous with clusters of small-sized and more irregularly shaped bubbles are also observed in comparison with that for a single tube. The bubbles departs at much higher frequencies and coalescence between two tubes. This phenomenon becomes more dominant and, with twin-tube arrangements, the sliding effect caused by the oncoming bubble from the lower tube surface obviously promotes nucleation of smaller size bubbles and activation of nucleation sites, especially at $q \geqslant 700$ W/m^2.

5.2. Boiling characteristics

Fig. 5 shows the nucleate boiling data for both increasing and decreasing mode for two twin-tubes arrangements with $p/d = 1.65$ and 2.5. Obviously, the lower tube has a larger degree of superheat (ΔT) for both arrangements. For instance, $(\Delta T)_{\text{upper tube}} \approx 1.8$ K $< (\Delta T)_{\text{lower tube}} \approx 2.8$ K at the same heat flux $q = 1000$ W/m^2 for $p/d = 1.65$ as shown in Fig. 5(a) with a decreasing heat flux mode. Moreover, the nucleate boiling curve shifts to the left as compared to that of single tube, indicating enhancement in heat transfer. Further inspection of Fig. 5(a) and (b), it is also found that an early onset of nucleate boiling was observed for $p/d = 2.5$ in comparison with that for $p/d = 1.65$, which strongly suggests a better heat transfer performance for $p/d = 2.5$ tube arrangement. The present boiling curves are experienced with an appreciable boiling hysteresis about 0.4–0.8 K especially for the upper tube for $p/d = 2.5$ and $p/d = 1.65$, respectively, an effect which does not appear to have been reported previously in the literature. This is perhaps due to the temperature gradient associated with the upper tube so that the flow blockage would be occurred.

As previously stated, the heat transfer enhancement compared to the single tube was found to be large especially for the upper tube for both cases ($p/d = 1.65$ and 2.5) considered in Fig. 5 which is due to the bulk upward movement of the fluid and circulation as well as turbulent effect produced by rising vapor bubbles. More detailed reasons can be explained in the following: this

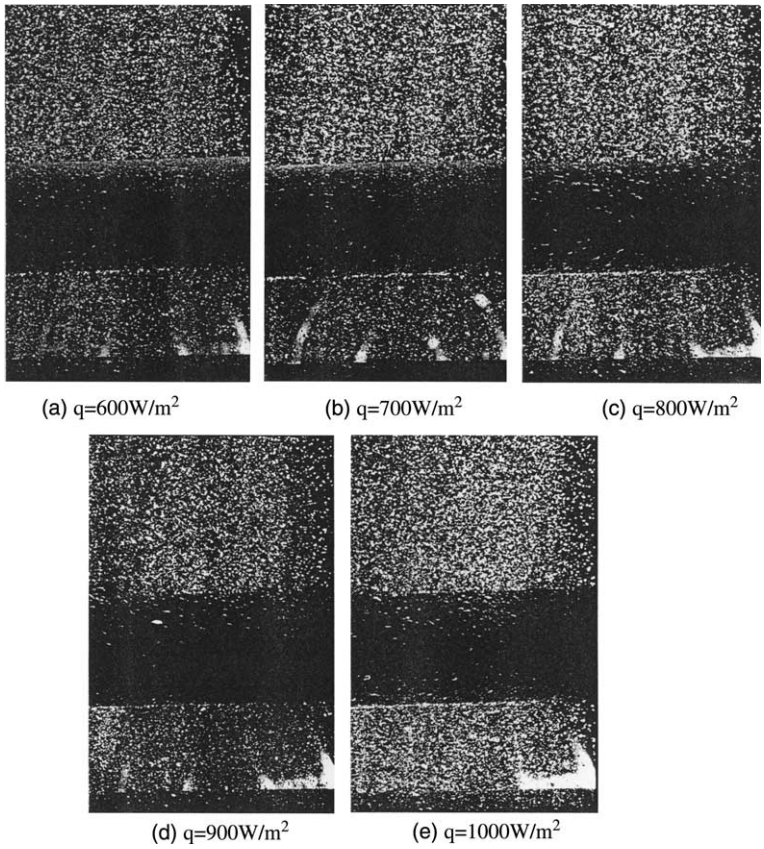

Fig. 4. Illustration of boiling visualizations.

may be due to the influence of the closely spaced tubes, but it should have an optimum p/d value as compared to the present results shown in Fig. 5(a) and (b), on the velocity and thermal fields in the wake region of a heated tube. Moreover, since the upper tube feel a warmer fluid caused by the lower tube. The warmer fluid decreases the local thermal driving potential which results in a poor nucleate boiling. However, at the same time, the upper tube are exposed to a moving fluid due to the lower tube. This move fluid enhances the convective heat transfer while the fluid evaporates. The counter-balanced effect is responsible for the afore-mentioned statements and it is dependent on the value of p/d.

5.3. Heat transfer coefficient

The heat transfer coefficients corresponding to Fig. 5 were plotted in Fig. 6. The data were reduced from the decreasing heat flux mode. Like boiling curves, the heat transfer coefficient curves again strongly exhibit the previous findings [13,16], the slope of these curves is about 0.64, which is a little bit lower than the traditional value ($\sim$0.7) for fully developed nucleate boiling due to the uncertainty of the experiments. Also included in Fig. 6 are the results from Browne and Bansal [13] and Hsieh and Ke [16] for comparison. As seen, the heat transfer coefficients of the lower tube for twin-tube arrangement of $p/d = 1.65$ being smaller than that for a plain tube of Browne and Bansal [13] for $q \leqslant 500$ W/m^2 which is in free convection regime. This is perhaps due to the boundary layer growth between the pores of the coating surface matrix. This is the same as previous findings of Hahne et al. [18].

The heat transfer enhancement can clearly be found as compared to the tube arrangements for $p/d = 1.65$ and 2.5. Such enhancement prevails in the entire heat flux levels (i.e., 100 W/m$^2 \leqslant q \leqslant 10$ kW/m^2). The reason for this is partly due to an increased agitation by a re-circulatory flow occurrence in the region in between two tubes and is partly due to the reasons which explained previously. Moreover, the mechanism which described the boiling process from porous structures of the present plasma coating surfaces can be explained as follows; it appears that the heat is conducted to a liquid vapor at the upper surface of the porous structure. This conduction supposedly occurs through the matrix (see Fig. 3

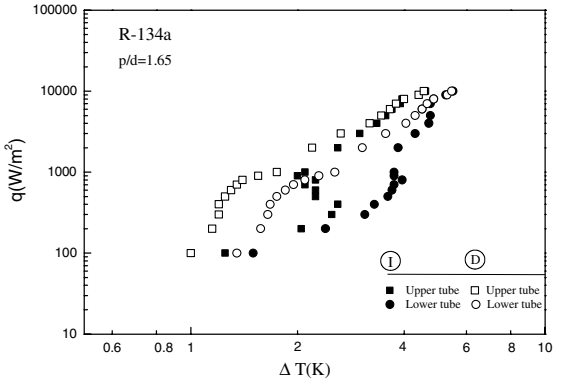

(a) p/d=1.65

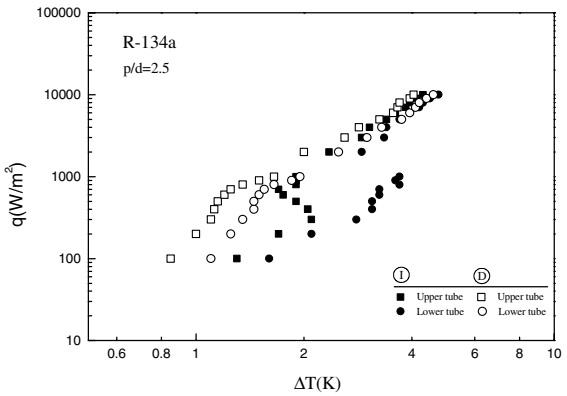

(b) p/d=2.5

Fig. 5. A typical boiling curve for the present study.

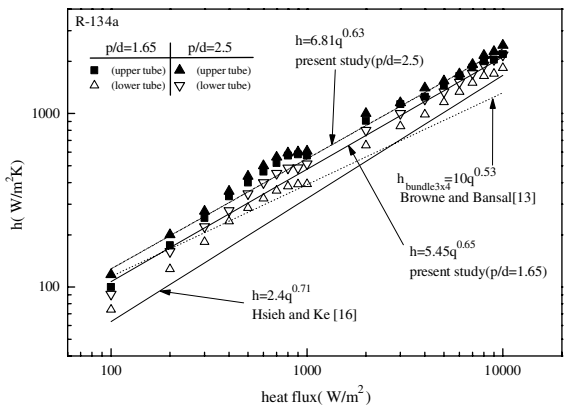

Fig. 6. Heat transfer coefficient as function of heat flux.

for details) formed by the solid portion of these wick and liquid in the porous spaces. It is recognized that the vapor bubbles exist within the pores formed by the void space between two solid portions. Heat is transferred by conduction through the solid matrix and then by conduction across the liquid portion. The pores within the matrix are interconnected so that liquid can be supplied to the pores and vapor can pass through the matrix to the free liquid surface. As vapor is generated within a pore, the pressure in the vapor bubble increases [17]. When the pressure is sufficiently high, it overcomes the surface tension retention force and the vapor if forced through the interconnected channels (pores) to the liquid surfaces. On the other hand, for wrapped tubes, since the additional nucleation sites were created and the cross-sectional area in the microstructure channel of the coated and smooth surface was reduced, the resulting boiling performances would be substantially improved.

Fig. 7 shows the experimental results for two plasma coated tubes arranged with two different pitches ($p/d = 1.65$ and 2.5). Following Hahne et al. [18], to show the effect of onflow to the upper tube, the ratio of the upper tube heat transfer coefficient to that of the lower tube was made. The results indicate that there exists two different trends for $p/d = 1.65$ and 2, respectively. The relative differences between the tube in different tubes pitches are different. It is seen that for $p/d = 1.65$ the ratio of the heat transfer coefficient of the upper and the lower tube is quite high. It is up to 1.5 at $q = 1000$ W/m^2. However, the situation is changed at $q = 300$ W/m^2 and rating $h_2/h_1 = 1.23$ for $p/d = 2.5$. Both h_2/h_1 gradually increase to the maximum and, then, decreases sharply. Again, however, for $p/d = 2.5$, the behavior looks moderate. Fig. 8 indicates the heat transfer enhancement for both upper and lower tubes relative to the single tube for all the heat flux levels considered. The single tube data were obtained from Hsieh and Ke [16] and Hsieh and Yang [17] for both single tubes. The heat transfer enhancement is clearly noted for both tube pitches. The enhancement value (h/h_s) ranged for 1.1 and 1.6 for $p/d = 1.65$ at $500 \leqslant q \leqslant 1000$ W/m^2. While for $p/d = 2.5$, such enhancement values can be up to 2.0. Generally, h/h_s

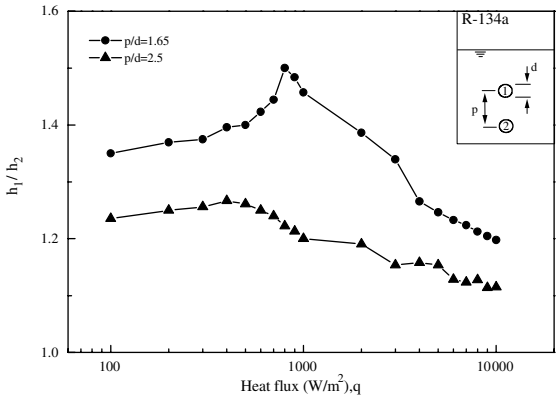

Fig. 7. h_1/h_2 vs. q.

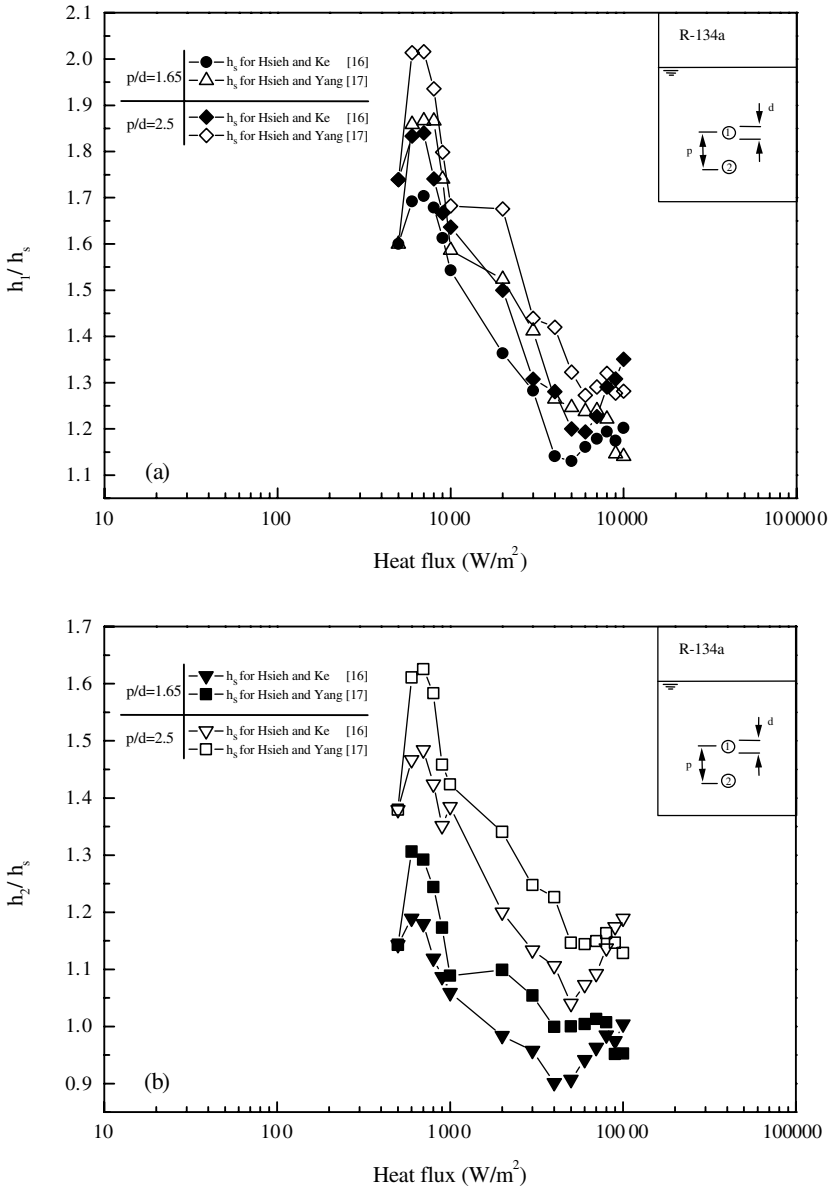

Fig. 8. h/h_s vs. q.

decreases as q increases. Under some circumstances, h/h_s is less than one ($=0.9$). The reason for this is that the bubble agglomeration occurs while $q \geqslant 3000$ W/m^2, which results in a poor heat transfer.

5.4. Bubble dynamic parameters (u, f, and d_b) for $p/d = 1.65$ twin-tube arrangement

The LDV system was used to determine an average of measured instantaneous bubble velocities at each height (see Fig. 1 for details) following Ammerman et al. [14] and Hsieh and Ke [16]. Fig. 9 indicates that the local bubble departure velocity along the bubble rising path above the lower and upper tubes, respectively at different heat flux levels ($600 \leqslant q \leqslant 1000$ W/m^2). For upper tube, local averaged bubble velocity increases along the rising path until a final velocity is approached at a height of 10 mm ($\sim$8 mm for single tube from Hsieh and Ke [16]) above the upper tube for all studied cases. However, unlike the single tube and the upper tube for the present twin-tube arrangement, such behavior for the lower tube did not occur due to the block of the upper tube causing a higher pressure there. Namely, the local bubble velocity gradually increases along the rising path

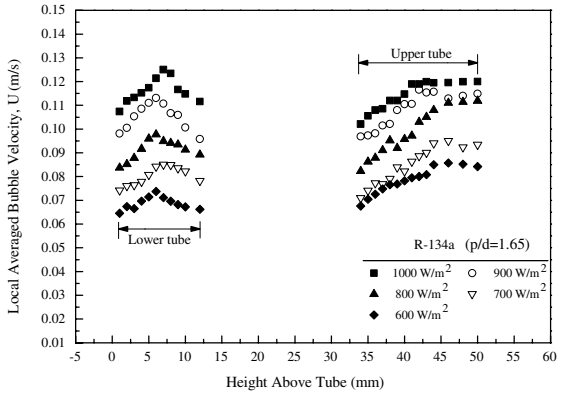

Fig. 9. Local averaged bubble velocity distribution vs. vertical position.

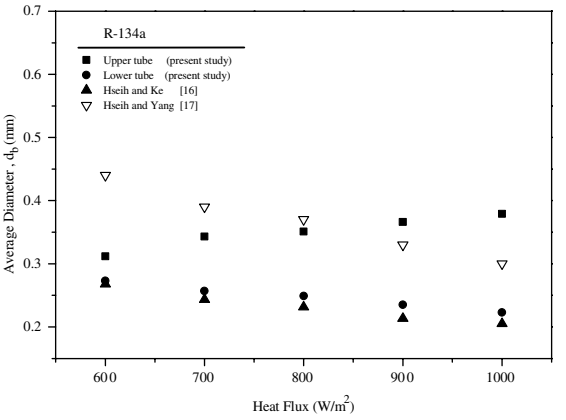

Fig. 11. Bubble diameter as function of heat flux.

to a position (about 5–6 mm above the lower tube) where the buoyancy force can not balance the drag force anymore, which results in a local bubble velocity decrease. Moreover, the values of the present velocity for the lower tube seem a little bit higher than those of single tube (about 5%).

Fig. 10 shows the frequency values vs. heat flux. Like single-tube results, the present twin-tubes results have the same trend, namely, the bubble departure frequency increases as the heat flux increases. However, the values for the upper tube are quite bigger as expected; while the values for the lower tube are somewhat smaller than those of single tube (data from Hsieh and Ke [16]) at $600 \leqslant q \leqslant 1000$ W/cm^2. The data in Fig. 11 indicate the bubble departure diameter distribution vs. heat flux. The different trend occurs for the upper/lower tubes. The lower tube data show that the bubble diameter slightly decreases as the heat flux increases which is the same as that for single tube, coincided with those from Hsieh and Ke [16] and Hsieh and Yang [17]. In fact, the present lower tube data is in good agreement with those of Hsieh and Ke [16]. Due to the bubble coalescence and agglomeration, $fd_b \cong$ constant is not found/valid for upper tube data.

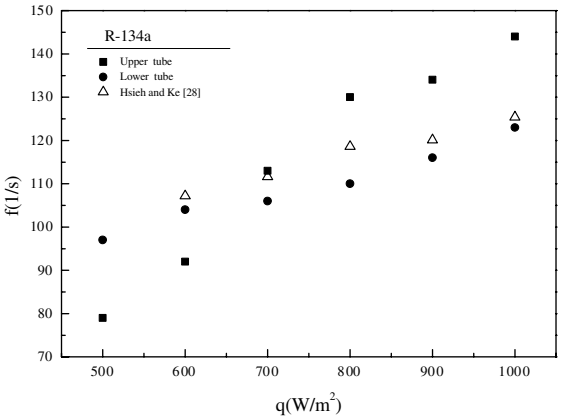

Fig. 10. Bubble departure frequency as function of heat flux.

5.5. Heat transfer mechanisms for the upper tube and modeling

The heat flux of the upper tubes is divided into a boiling and a convection heat flux following Hahne et al. [18]. The convection heat flux is caused by the onflow of a liquid vapor mixture coming from the boiling of the lower tube. Therefore, the convective heat transfer on the upper tube consists of a nucleate boiling part and on onflow part depending on the vapor flow flux. Boiling heat flux data can be obtained from Hsieh and Ke [16] for a single plasma coated tube for the same condition. The onflow part included q_{cb}, q_{cs} and q_{ct} three parts for tube bottom, side and top surface. The area ratios of A_b/A, A_s/A, and A_t/A are 0.1, 0.8, and 0.1 by observation at $p/d = 1.65$ of the present study (see Table 3 for details).

After careful calculations, it is found that Hahne et al. [18] model can also be applied to the present plasma coated twin-tubes arrangements. The percentage for the onflow vapor flux contribution can be clearly seen in Table 4. Also listed in Table 4 is the single-tube results. As you can see, for a single tube, q_b, nucleate boiling

Table 3
A_b/A, A_s/A and A_t/A details

Tube pitch	A_b/A	A_s/A	A_t/A
1.65	0.07	0.86	0.07

Note: A: 12 874 mm^2; A_b: 901.18 mm^2; A_s: 11 071.64 mm^2; A_t: 901.18 mm^2.

Table 4
Relative percentage of the heat flux due to different heat transfer mechanism

Tubes arrangement	Heat flux (W/m^2)	Percentage of heat flux (%)				
		q_b	q_{cb}	q_{cs}	q_{ct}	q_{fc}
Twin-tubes arrangement ($p/d = 1.65$)	600	25.3	49.1	20.1	5.6	
	700	21.5	53.9	18.3	6.3	
	800	18.0	60.2	14.7	7.1	
	900	15.7	62.7	14.4	7.2	
	1000	14.7	63.5	14.4	7.4	
Single tube	600	74.2				25.8
	700	77.3				22.7
	800	78.1				21.9
	900	80.8				19.2
	1000	81.9				18.1

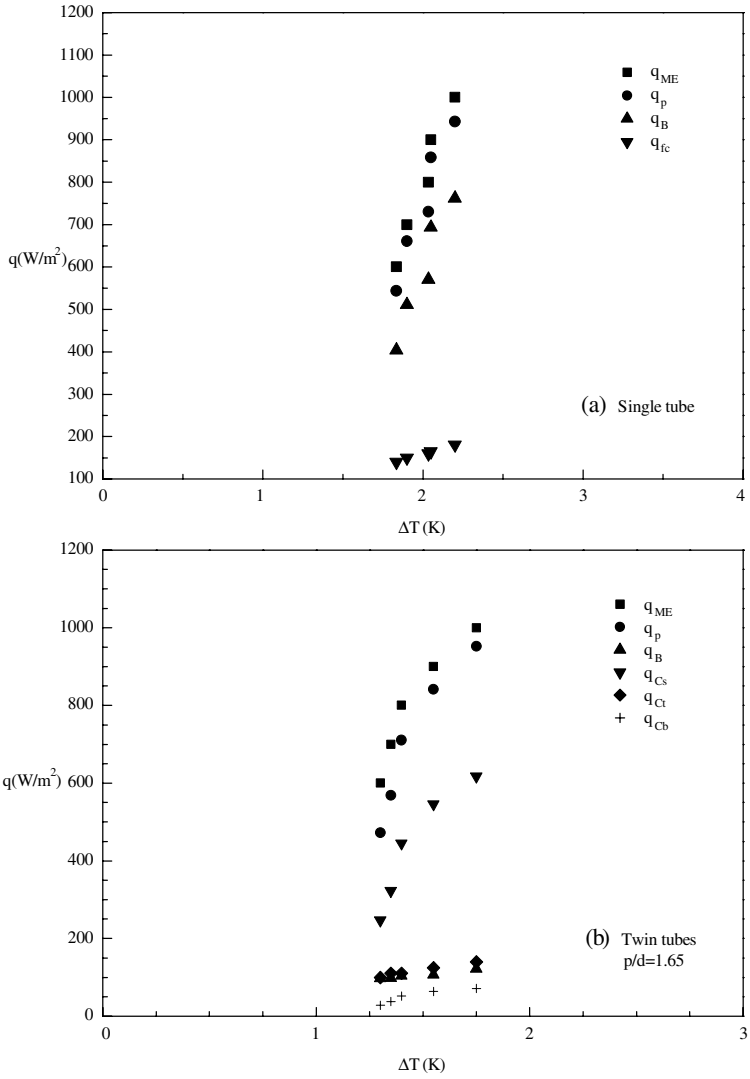

Fig. 12. Comparison of the model with the experimental data for R-134a.

heat flux increases as the heat flux increases as one would expect. However, such behavior does not happen for twin-tubes arrangements as in Fig. 12(a) and (b), respectively. On the contrary, heat flux due to the onflow vapor flux takes most part. In fact, q_b decreases as q increases. Among the three (i.e., q_{cb}, q_{cs}, q_{ct}) contribution, q_{cb} increases as the heat flux increases. Fig. 12 by plotting these data from Table 4 also illustrates such results. In addition, based on Fig. 12, the calculated heat flux (q_p) is in good agreement with those from measurements for both single tube and twin-tubes arrangements as shown in Fig. 12(a) and (b), respectively. In short, for twin-tubes arrangements, the major heat transfer mechanism comes from the onflow vapor flux convection. It was found that such effect can be up to 85% at $q = 1000$ W/m^2 and $p/d = 1.65$ (Table 4). Such value would expect to be higher as the heat flux flux q increases further.

6. Conclusion

Pool nucleate boiling data from twin plasma coated tubes in saturated R-134a at low and machete heat flux for $p/d = 1.65$ and 2.5 with LDV assisted bubble dynamic parameters for $p/d = 1.65$ were presented and discussed to study the p/d and tubes arrangements effect on heat transfer performance. The results lead to the following conclusions.

1. An appreciable boiling hysteresis was found to be occurred for the upper tube as compared to that of low tube in a twin-tube arrangement.
2. Local bubble velocity distribution along its rising path was found. Unlike Hsieh and Ke [16], a final velocity can not be found for the lower tube for the present two-tubes arrangements. In addition, the magnitude of the present study seems a little bit higher ($\sim$5% higher) than that of single tube.
3. For bubble departure frequency vs. heat flux distribution, twin-tube results are consistent with those of single tubes. However, the values of the upper tube are considerable higher. While, for bubble departure diameter, the upper/lower tube show different trend with heat flux.
4. Following Hahne et al. [18], present results can be modeled through so called onflow vapor flux mechanism. Again, the present demonstrates for an upper tube of the twin-tubes arrangements the dominant heat transfer mechanism is not nucleate boiling. While the major part, comes from onflow vapor flux. It is proved that such values can be up to 85% for the present study of $p/d = 1.65$ at $q = 1000$ W/m^2. The results also indicate that such values can be even higher as q increases.

References

[1] J.W. Palen, J.J. Taborek, Refinery kettle reboilers-proposed method for design and optimization, Chem. Eng. Prog. 58 (1962) 37–46.
[2] J.W. Palen, W.M. Small, New way to design kettle and internal reboilers, Hydrocarb. Process. 43 (1963) 199–208.
[3] J.W. Palen, A. Yarden, J. Taborek, Characteristics of boiling outside large-scale horizontal multitube bundles, AIChE Symp. Ser. 68 (1972) 50–61.
[4] L.S. Leong, K. Cornwell, Heat transfer coefficients in a reboiler tube bundle, Chem. Eng. 20 (1979) 219–221.
[5] K. Cornwell, R.B. Schuller, A study of boiling outside a tube bundle using high speed photography, Int. J. Heat Mass Transfer 25 (1982) 683–690.
[6] M.K. Jensen, J.T. Hsu, A parametric study of boiling heat transfer in a horizontal tube bundle, ASME J. Heat Transfer 110 (1988) 976–981.
[7] Y. Fujita, H. Ohta, S. Hidaka, K. Nishihawa, Nucleate boiling heat transfer on horizontal tube in bundles, in: Proceedings of Eighth International Heat Transfer Conference, San Francisco, vol. 5, 1986, pp. 2131–2136.
[8] J. Muller, Boiling heat transfer on finned tube bundles: the effect of tubes position and intertube spacing, in: Proceedings of Eighth International Heat Transfer Conference, San Francisco, vol. 5, 1986, pp. 2111–2116.
[9] M.K. Jensen, R.R. Trewin, A.E. Bergles, in: V.K. Dhir, A.E. Bergles (Eds.), Crossflow Boiling in Enhanced Tube Bundles, Pool and External Flow Boiling, ASME, 1992, pp. 373–379.
[10] P.J. Marto, C.L. Anderson, Nucleate boiling characteristics of R-113 in a small tube bundle, ASME J. Heat Transfer 114 (1992) 425–433.
[11] S.B. Memory, S.V. Chilman, P.J. Marto, Nucleate pool boiling of a TURBO-B bundle in R-113, ASME J. Heat Transfer 116 (1994) 670–677.
[12] Z.-X. Li, E. Hahne, Boiling heat transfer on finned tube bubble with lower tubes heated with constant heat flux, Exp. Therm. Fluid Sci. 11 (1995) 174–180.
[13] G. Barthau, Active nucleate site density and pool boiling heat transfer—an experimental study, Int. J. Heat Mass Transfer 35 (1992) 271–278.
[14] C.-N. Ammerman, S.-M. You, Y.-S. Hong, Identification of pool boiling heat transfer mechanisms from a wire immersed in saturated FC-72 using a single-photo/LDA method, ASME J. Heat Transfer 118 (1996) 117–123.
[15] R. Mertz, M. Groll, Ch. Marvillet, J.E. Hesselgreaves, Enhanced static heat transfer surfaces for compact two-phase heat exchangers, Heat Recov. Syst. CHP 14 (1994) 493–506.
[16] S.S. Hsieh, C.G. Ke, Bubble dynamic parameters and pool boiling heat transfer on plasma coated tubes in saturated R-134a and R-600a, ASME J. Heat Transfer 124 (2002) 704–716.
[17] S.S. Hsieh, T.-Y. Yang, Nucleate pool boiling from coated and spirally wrapped tubes in saturated R-134a and R-600a at low and moderate heat flux, ASME J. Heat Transfer 123 (2001) 257–270.
[18] E. Hahne, Q.-R. Chen, R. Windisch, Pool boiling heat transfer on finned tube—an experimental and theoretical study, Int. J. Heat Mass Transfer 34 (1991) 2071–2078.